Available online at www.sciencedirect.com

ScienceDirect

International Journal of Solids and Structures 44 (2007) 8213–8228

INTERNATIONAL JOURNAL OF SOLIDS AND STRUCTURES

www.elsevier.com/locate/ijsolstr

Micromechanical modeling of packing and size effects in particulate composites

V. Marcadon [a,*], E. Herve [b], A. Zaoui [a]

[a] *Laboratoire de Mécanique des Solides, Ecole Polytechnique, C.N.R.S UMR 7649, F-91128 Palaiseau Cedex, France*
[b] *Laboratoire d'Ingénierie des Systèmes de Versailles, Université de Versailles Saint-Quentin en Yvelines, 45 Avenue des Etats-Unis, F-78035 Versailles Cedex, France*

Received 5 April 2007; received in revised form 23 May 2007; accepted 13 June 2007
Available online 15 June 2007

Abstract

This paper is devoted to the introduction of packing and size effects in micromechanical predictions of the overall elastic moduli of particulate composite materials. Whereas micromechanical models derived from the classical 'point approach' are known to be unable to model such effects, it is shown that the so-called 'morphologically representative pattern-based approach' (MRP-based approach) offers new means of taking some geometrical parameters into account such as the mean distance between nearest-neighbor particles or their size, so as to predict the dependence of the overall moduli on these parameters, at least in a relative way. Moreover, when internal lengths, such as the thickness of interphase shells of coated particles, are introduced, absolute size effects can be predicted as well. Illustrative applications are reported in view of comparisons between such new treatments and the predictions of some classical models which are shown to coincide with the ones derived from MRP-based models in definite limiting cases only.

Keywords: Spherical particles; Packing effect; Size effect; Micromechanical models; Particulate composites

1. Introduction

The current development of nanocomposites has drawn increased attention on particle or fiber size effects on their overall elastic moduli: at fixed volume fraction, an overall stiffening effect is commonly expected from the smaller particle size and the associated decrease of the mean distance between particles or the increase of the interfacial area. Whereas modeling approaches for such effects are mainly searched in the framework of percolation theory, of second-gradient techniques or of generalized continua theory, it is considered that Eshelby-type micromechanical models are definitely unable to capture any size effect: obviously, no length scale exists in the inclusion-infinite matrix basic Eshelby problem and the same statement holds for all the

* Corresponding author. Present address: ONERA - DMMP, 29 Avenue de la Division Leclerc, BP 72, F-92322 Châtillon Cedex, France. Tel.: +33 146734524; fax: +33 146734164.
E-mail address: Vincent.Marcadon@onera.fr (V. Marcadon).

0020-7683/$ - see front matter
doi:10.1016/j.ijsolstr.2007.06.008

current 2-point correlation-based bounds and estimates, which are frequently expressed through (or derived from) the solution of various Eshelby-type problems. This is not only the case for the Hashin–Shtrikman bounds (Hashin and Shtrikman, 1963), but also for all the Hashin–Shtrikman estimates, including the classical self-consistent scheme (Kröner, 1978), as well as for the three-phase model (Christensen and Lo, 1979), the Mori-Tanaka model (Mori and Tanaka, 1973), the n-phase model (Hervé and Zaoui, 1993), etc.

The main reason for that lies in the fact that all these models derive from what can be called 'point-approaches', according to which the Representative Volume Element (RVE) is defined through some statistical information on points belonging to such or such phase. Consequently, when the resulting bounds or estimates for the overall properties are found to be obtainable from the solution of some inclusion-matrix problem, the inclusions (as well as the shells for the case of composite inclusions, such as for the n-phase model) are only abstract representatives of a phase—*e.g.*, the set of all grains with the same lattice orientation for a polycrystal or the whole reinforcing phase for a composite material—and are in no way physical individual particles, fibers, phase domains or grains. Thus, it is meaningless to endow them with any individual geometrical or physical specific property of these phase elements, such as their size, their mutual distances or their superficial area.

At variance with these 'point approaches', more recently developed 'pattern approaches' yield alternative treatments which potentially allow such properties to be taken into account. This is the case with the so-called 'morphologically representative pattern-based approach' (Stolz and Zaoui, 1991), referred to as the 'MRP-based approach' in the sequel, which derives from the basic idea of Hashin's Composite Sphere Assemblage (CSA (Hashin, 1962)): according to the CSA, finite composite spheres (instead of points) are identified in the RVE. This idea can be generalized by considering several sets of identical composite domains (the 'patterns') with arbitrary but known material content: from statistical information on the spatial distribution of these patterns, new bounds and estimates can be derived for the overall elastic properties (Bornert et al., 1996). Unlike the classical 'mechanical phases' which differ from each other by their mechanical properties, the considered patterns, which play the role of 'morphological phases', now give access to individual particles or domains, with their own specific attributes such as their size or their superficial area.

This paper aims at exploring, by use of classical methods of continuum micromechanics, the capacity of the MRP-based approach to tackle some phenomena which are commonly considered as lying out of reach of these methods, such as packing and size effects in composites. For the sake of simplicity, only isotropic elastic composites with isotropically distributed monodisperse spherical particles are considered, though indications are given in time on the way to deal with more general situations. After a brief survey of the MRP-based approach (Section 2), this method is specified for the problems under investigation and illustrated for modeling packing effects (Section 3). Internal lengths are then taken into account in more detail, in view of the prediction of size effects (Section 4), with special emphasis on the influence of the presence of an 'interphase', *i.e.*, of interfacial zones between the inclusions and the matrix: whereas classical or modified Eshelby-type models can only be considered as able to treat limiting cases (Section 5), the MRP-based approach yields a general modeling tool, whose predictions, compared with those derived from other models, are illustrated for various situations in Section 6.

Most of the used notations are quite classical; vectors and second-order tensors are underlined once and twice, respectively; fourth-order tensors are indicated with bold characters.

2. The MRP-based approach

The main elements of this approach can be summed up as follows (for more details, see, *e.g.*, Bornert et al., 1996). It is first assumed that the RVE can be decomposed into a set of P families of identical finite composite domains whose material content is known, the 'patterns', say $D_\lambda, \lambda \in [1, P]$, with the volume fraction c_λ and the elastic moduli $\mathbf{C}_\lambda(\underline{x})$: this microstructure can be referred to as a generalized Hashin's assemblage of patterns. If the patterns do not fill completely the RVE and the surrounding domain D_0 is occupied by a single homogeneous phase, the 'matrix', with the volume fraction c_0 and the moduli $\mathbf{C}_0$, this domain D_0 can be considered as an additional pattern. In each pattern (λ), one can consider 'homologous points', *e.g.*, the pattern centers $\underline{X}_\lambda^k$, which have the same relative location in the N_λ different domains D_λ^k, $k \in [1, N_\lambda]$ (see Fig. 1).

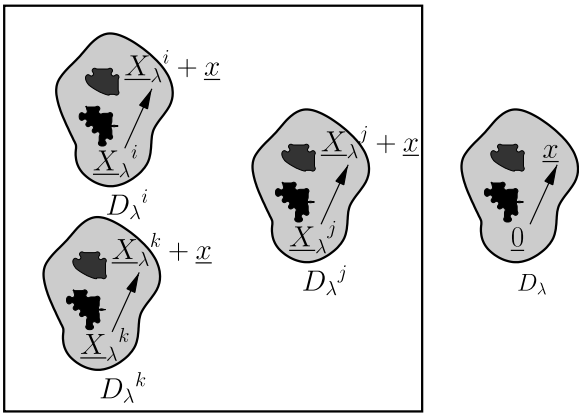

Fig. 1. A morphologically representative pattern.

For homogeneous boundary conditions on the RVE, generalized Voigt–Reuss type bounds can be easily derived by transferring these conditions on the boundary of each domain D_λ^k. In the surrounding matrix, classical homogeneous trial strain and stress fields are used. From the (either analytical or numerical) computation of the corresponding solutions, the Voigt-type and Reuss-type bounds derive from homogeneous strain and stress boundary conditions, respectively.

Sharper bounds or estimates for the effective properties can be derived by using, in the classical Hashin–Shtrikman variational approach (Hashin and Shtrikman, 1963), a nonuniform polarization field $\underline{\underline{p}}^*$ within the domains, taking the same value at homologous points of every pattern, and a classical homogeneous polarization field $\underline{\underline{p}}_0^*$ in the matrix outside the patterns. These fields generate strain and stress fields on a fictitious homogeneous reference medium with arbitrary elastic moduli $\mathbf{C}^0$ and the same geometry and boundary conditions as the actual RVE, which can be used as admissible trial fields for the initial problem. The Hashin–Shtrikman functional HS^0 then yields upper and lower bounds for the effective linear strain energy $W(\underline{\underline{E}})$ of the initial problem, with $\underline{\underline{E}}$ the macroscopic strain, for any choice of $\underline{\underline{p}}^*$ as soon as the moduli $\mathbf{C}^0$ are chosen such that $\delta\mathbf{C}^0 = [\mathbf{C}(x) - \mathbf{C}^0]$ is everywhere negative or positive definite, respectively.

Under the assumption of macrohomogeneity, the local stress and strain fields can be derived from the use of Green techniques relative to an infinite body. Optimal bounds are obtained when the polarization fields make the functional HS^0 maximal and minimal. A convenient way to derive explicit bounds relies on the definition of 'pattern-based average values', say $g_\lambda^M(\underline{x})$ for pattern (λ), which are associated with any field $g(\underline{x})$ in the RVE through

$$g_\lambda^M(\underline{x}) = \frac{1}{N_\lambda}\sum_{k=1}^{N_\lambda} g(\underline{x} + \underline{X}_\lambda^k), \quad \forall\lambda. \tag{1}$$

Optimal polarization fields $\underline{p}$ are such that $\underline{p}_\lambda(\underline{x}) = (\mathbf{C}_\lambda(\underline{x}) - \mathbf{C}^0) : \underline{\underline{\varepsilon}}(\underline{p})_\lambda^M(\underline{x}), \forall \underline{x} \in D_\lambda$, for all patterns (λ) and $\underline{p}_0 = (\mathbf{C}_0 - \mathbf{C}^0)$: $<\underline{\underline{\varepsilon}}(\underline{p})>_0$, where $<\underline{\underline{\varepsilon}}(\underline{p})>_0$ is the average of $\underline{\underline{\varepsilon}}(\underline{p})$ in the matrix outside the patterns.

In view of the application of this theory to the problems addressed below, the main practical result is the following (Bornert et al., 1996): under the hypothesis of an ellipsoidal distribution of the domain centers, the resulting optimized pattern-based strain averages are the solution of Eshelby-type inhomogeneity problems where the infinite matrix, subjected to the same uniform strain $\underline{\underline{\varepsilon}}_0$ at infinity, has the moduli $\mathbf{C}^0$ and the ellipsoidal composite inhomogeneities are the different (ellipsoidal) patterns by turn, the possible surrounding matrix being itself treated as a homogeneous pattern with same shape. Note that for the isotropic distribution of pattern centers considered hereafter, a consistent and in some sense optimal description of the microstructure requires the patterns outer shape D_λ to be all spherical. As soon as these pattern-based strain averages have been derived from the solution of these inhomogeneity problems, the generalized Hashin–Shtrikman tensor of elastic moduli $\mathbf{C}_{\mathrm{MRP}}^{\mathrm{HS}}$, obtained with reference medium $\mathbf{C}^0$, is identified from the relations

$$\forall \underline{\underline{E}}, \qquad \mathbf{C}^{\mathrm{HS}}_{\mathrm{MRP}}(\mathbf{C}^0) : \underline{\underline{E}} = \sum_{\lambda=0}^{P} c_\lambda < \mathbf{C}_\lambda : \underline{\underline{\varepsilon}}^M_\lambda >_{D_\lambda}. \tag{2}$$

It is an upper or a lower bound of the effective moduli when $\mathbf{C}^0$ is chosen as specified above. Alternatively, generalized self-consistent estimates $\mathbf{C}^{\mathrm{SC}}_{\mathrm{MRP}}$ are defined as the solution of the implicit equation $\mathbf{C}^{\mathrm{HS}}_{\mathrm{MRP}}(\mathbf{C}^{\mathrm{SC}}_{\mathrm{MRP}}) = \mathbf{C}^{\mathrm{SC}}_{\mathrm{MRP}}$, which can be solved iteratively.

When applied to the classical CSA, where all the composite spheres with the same diameter define one pattern, and under the assumption of an isotropic distribution of the sphere centers, the various resulting Eshelby-type problems are identical and new Hashin–Shtrikman-type bounds and estimates are easily derived analytically (Hervé et al., 1991); the corresponding MRP-based self-consistent estimate is shown to coincide with the three-phase model (Christensen and Lo, 1979). For the isotropic generalized CSA, with several families of patterns, one Eshelby-type problem can be associated with each family of patterns: these problems must be solved either numerically when the spherical domains content is arbitrary (Bornert et al., 1996) or analytically for simpler geometry, as shown below. Note that when a residual surrounding matrix D_0 exists, as below, its own auxiliary Eshelby-type problem reduces to the classical Eshelby problem. In what follows, for ease of notation, the superscript M used for the definition of the 'pattern-based average values' in Eq. (1) is omitted.

3. Packing effects

The MRP-based approach can be used for the investigation of the influence of the distance between particles on the overall properties of an elastic isotropic composite composed of a continuous matrix and isotropically dispersed spherical particles with the same radius R_{inc}. The CSA, which needs the whole space of the RVE to be filled up with similar composite spheres, is obviously irrelevant to such a morphology since the particles and then the composite spheres cannot have a vanishing size. The classical models derived from the 'point approach' cannot integrate the property of particle monodispersity either. According to the MRP-based approach, spherical shell-core patterns can be defined, each pattern consisting of one particle surrounded by a concentric shell of matrix of variable thickness depending on the packing density, with an additional pattern of residual pure matrix. The shell thickness may then be correlated with the mean distance between nearest-neighbor particles, say λ. For Torquato (1995), this mean distance is a statistical variable which can be estimated and bounded. Its distribution function, say $\phi(\lambda)$, is supposed to be known here; it can be discretized into a finite number P of discrete values $\phi_\mu, \mu \in [1,P]$ with $\sum_\mu \phi_\mu = 1$, associated with the shell thickness $\lambda_\mu/2$. For a given volume fraction f_1 of the particles in the composite, the volume fractions of the composite patterns c_μ and of the additional matrix pattern c_0 can easily be found as

$$\left.\begin{aligned} c_\mu &= f_1 \phi_\mu \left(1 + \tfrac{\lambda_\mu}{2R_{\mathrm{inc}}}\right)^3 \\ c_0 &= 1 - f_1 \sum_\mu \phi_\mu \left(1 + \tfrac{\lambda_\mu}{2R_{\mathrm{inc}}}\right)^3. \end{aligned}\right\} \tag{3}$$

Bounds and estimates for the effective moduli of the composite can then be derived according to the method presented in Section 2 for this $(P+1)$-pattern approach by using the solution of the auxiliary 'Problem [P]' of a composite sphere embedded in an infinite homogeneous matrix which is recalled in Appendix A. From these equations and formulae (3), it is apparent already that the effective properties simultaneously depend on the particle size R_{inc} and on the packing parameters λ_μ through the ratios $(\lambda_\mu/R_{\mathrm{inc}})$ so that the resulting size effect can be appreciated in advance as a relative one only.

In view of illustration, one single packing parameter λ is considered now, for the sake of simplicity. So, two spherical patterns only have to be considered: with the notations of Appendix A, the first pattern is made of two concentric spheres, with a particle at the core (radius $R_1 = R_{\mathrm{inc}}$) and a shell, with the thickness $R_2 - R_1 = \lambda/2$, constituted with the pure matrix material. The second pattern is filled with the matrix material only. So, $P = 1$, $\phi_1 = 1$, $\lambda_1 = \lambda$ and $c_1 = f_1(1 + \lambda/2R_{\mathrm{inc}})^3$. The type of packing can be characterized by this c_1 value, which is also the maximum value of the particle volume fraction, say $f_1^{\max}$, which can be reached for this

type of packing (*i.e.*, for $\lambda = 0$). Note that, for crystallographic lattices, c_1 and then $f_1^{\max}$ have well-known definite values ($\pi\sqrt{2}/6 \approx .74$, $\pi\sqrt{3}/8 \approx .68$, $\pi/6 \approx .52$, etc. for face-centered, body-centered and simple cubic lattices, respectively) whereas a continuous variation of c_1 can be considered for the isotropic packings studied here.

Within this simplified 'two-pattern' approach, two auxiliary problems only must be solved, by embedding each pattern in an infinite homogeneous elastic matrix with adequate moduli subjected to the same uniform strain at infinity. The investigation is restricted here to the generalized self-consistent prediction of the effective moduli as a function of f_1 for different values of c_1. This prediction is then derived from the solution of two elementary problems: the first one is given in Appendix A and the second one is the classical Eshelby's solution for a spherical inhomogeneity, with in both cases the infinite fictitious matrix constituted with the effective medium (*i.e.*, the "Homogeneous Equivalent Medium", HEM) and the auxiliary strain at infinity $\underline{\underline{\varepsilon}}_0$ to be determined from the condition $\underline{\underline{E}} = <\underline{\underline{\varepsilon}}>$ (Fig. 2). Note that whereas Eshelby-based classical micromechanical models would have been unable to capture any packing effect by themselves, the solution of Eshelby-type problems, when integrated within the MRP-based approach, provides a key tool for modeling this effect.

The relative volume fraction of the particle in pattern (1) is $f_1/c_1 = (R_1/R_2)^3$. Let $\underline{\underline{\varepsilon}}_j^{(\lambda)}$ denote the average strain of phase (j) inside pattern (λ), with $\lambda \in [1,2]$, $j \in [1,2]$. Since the elasticity is linear without eigenstrains, the overall average strains $\underline{\underline{\varepsilon}}_j$ read simply

$$\underline{\underline{\varepsilon}}_j = \mathbf{A}_j : \underline{\underline{E}} \tag{4}$$

where the fourth-order tensors $\mathbf{A}_j$ are the average strain concentration tensors for phase (j) and the effective moduli $\mathbf{C}^{\text{eff}}$ are derived from the classical relations

$$\mathbf{C}^{\text{eff}} = <\mathbf{C} : \mathbf{A}> = \sum_j f_j \mathbf{C}_j : \mathbf{A}_j \tag{5}$$

with $\mathbf{C}_j$ the phase moduli. On the other hand, the considered auxiliary problems yield the solutions $\underline{\underline{\varepsilon}}_j^{(\lambda)}$, related to $\underline{\underline{\varepsilon}}_0$ through the fourth-order tensors $\mathbf{A}_j^{(\lambda)}$:

$$\underline{\underline{\varepsilon}}_j^{(\lambda)} = \mathbf{A}_j^{(\lambda)} : \underline{\underline{\varepsilon}}_0 \tag{6}$$

so that we get for the per phase average strains $\underline{\underline{\varepsilon}}_j$:

$$\underline{\underline{\varepsilon}}_j = \sum_\lambda c_\lambda \mathbf{A}_j^{(\lambda)} : \underline{\underline{\varepsilon}}_0 = \left(c_1 \mathbf{A}_j^{(1)} + c_2 \mathbf{A}_j^{(2)}\right) : \underline{\underline{\varepsilon}}_0. \tag{7}$$

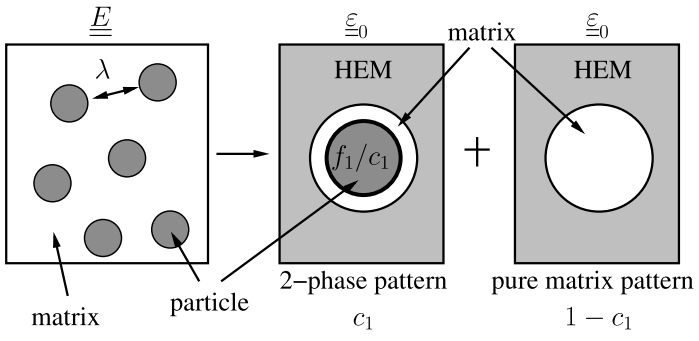

Fig. 2. Packing effect modelled with a 2-pattern approach.

The average concentration tensors $\mathbf{A}_j$ can then be obtained as follows:

$$\left.\begin{aligned}
&\underline{\underline{E}} = <\underline{\underline{\varepsilon}}> = \sum_j f_j \underline{\underline{\varepsilon}}_j = \sum_j f_j \left(\sum_\lambda c_\lambda \mathbf{A}_j^{(\lambda)} \right) : \underline{\underline{\varepsilon}}_0 \\
&\underline{\underline{\varepsilon}}_0 = \left(\sum_j f_j \left(\sum_\lambda c_\lambda \mathbf{A}_j^{(\lambda)} \right) \right)^{-1} : \underline{\underline{E}} \\
&\mathbf{A}_i = \sum_\lambda c_\lambda \mathbf{A}_i^{(\lambda)} : \left(\sum_j f_j \left(\sum_\lambda c_\lambda \mathbf{A}_j^{(\lambda)} \right) \right)^{-1}
\end{aligned}\right\} \tag{8}$$

where the last equation in Eq. (8) derives from the combination of Eqs. (4) and (7). The effective moduli $\mathbf{C}^{\text{eff}}$ are then obtained by Eq. (5).

Since the considered situation is fully (*i.e.*, both mechanically and geometrically) isotropic, the concentration tensors $\mathbf{A}_j$ and $\mathbf{A}_j^{(\lambda)}$ are isotropic too and they can be decomposed on the projectors $\mathbf{J} = \frac{1}{3}\underline{\underline{i}} \otimes \underline{\underline{i}}$ and $\mathbf{K} = \mathbf{I} - \mathbf{J}$ on the subspaces of purely spherical and deviatoric second-order tensors, respectively, with $\underline{\underline{i}}$ and $\mathbf{I}$ the second- and fourth-order identity tensors:

$$\left.\begin{aligned}
&\mathbf{A}_j = A_{dj}\mathbf{K} + A_{sj}\mathbf{J} \\
&\mathbf{A}_j^{(\lambda)} = A_{dj}^{(\lambda)}\mathbf{K} + A_{sj}^{(\lambda)}\mathbf{J}
\end{aligned}\right\} \tag{9}$$

where A_{dj}, A_{sj}, $A_{dj}^{(\lambda)}$ and $A_{sj}^{(\lambda)}$ are simple scalars.

According to the results of Appendix A, we have for pattern (1) ($\lambda = 1$), with $\mu_3 = \mu^{\text{eff}}$, $v_3 = v^{\text{eff}}$ and $k_3 = k^{\text{eff}}$ in Eqs. (23) and (24):

$$A_{dj}^{(1)} = a_{dj}, \qquad A_{sj}^{(1)} = a_{sj}, \quad j \in [1,2] \tag{10}$$

whereas for pattern (2), which simply refers to Eshelby's problem, the classical solution reads

$$\left.\begin{aligned}
&A_{d1}^{(2)} = A_{s1}^{(2)} = 0 \\
&A_{d2}^{(2)} = 1 + \beta^{\text{eff}} \tfrac{\mu_2 - \mu^{\text{eff}}}{\mu^{\text{eff}}}, \qquad A_{s2}^{(2)} = 1 + \alpha^{\text{eff}} \tfrac{k_2 - k^{\text{eff}}}{k^{\text{eff}}} \\
&\beta^{\text{eff}} = \tfrac{6(k^{\text{eff}} + 2\mu^{\text{eff}})}{5(3k^{\text{eff}} + 4\mu^{\text{eff}})}, \qquad \alpha^{\text{eff}} = \tfrac{3k^{\text{eff}}}{3k^{\text{eff}} + 4\mu^{\text{eff}}}
\end{aligned}\right\} \tag{11}$$

From Eqs. (8) and (9), the average concentration tensors $\mathbf{A}_j$ derive from

$$A_{di} = \frac{\sum_\lambda c_\lambda A_{di}^{(\lambda)}}{\sum_j f_j \left(\sum_\lambda c_\lambda A_{dj}^{(\lambda)} \right)}, \qquad A_{si} = \frac{\sum_\lambda c_\lambda A_{si}^{(\lambda)}}{\sum_j f_j \left(\sum_\lambda c_\lambda A_{sj}^{(\lambda)} \right)} \tag{12}$$

and, according to the decomposition $\mathbf{C} = 2\mu\mathbf{K} + 3k\mathbf{J}$ and to Eq. (5), the effective moduli are given by

$$\mu^{\text{eff}} = f_1\mu_1 A_{d1} + f_2\mu_2 A_{d2}, \qquad k^{\text{eff}} = f_1 k_1 A_{s1} + f_2 k_2 A_{s2}. \tag{13}$$

The associated variation of the normalized effective moduli with respect to the particle volume fraction f_1 is illustrated in Fig. 3 for a two-pattern (generalized) self-consistent scheme and several values of c_1. Whereas, for the limit value $c_1 = 1$, a CSA-type behavior is obtained, the predictions of the classical self-consistent scheme (SCS) are recovered for $c_1 = f_1$, *i.e.*, for $f_1 = f_1^{\max}, \forall c_1$: this was of course expected from the fact that the shell thickness then vanishes. Here again, the exhibited size effect is only a relative one since the particle radius R_{inc} is always scaled by the packing distance λ: for a given volume fraction f_1 and a fixed value of λ, the stiffening efficiency of the particles, which is minimum for the CSA, is increasing with the particle size.

Finally, it can be noticed that the situation depicted at the beginning of this section for monodisperse particles and several packing parameters λ_μ can be interpreted as well as the case of a composite with several particle diameters and one packing parameter or of any intermediate configuration with various particle size and packing parameters described by the distribution function of the dimensionless variable (λ/R_{inc}). It is apparent

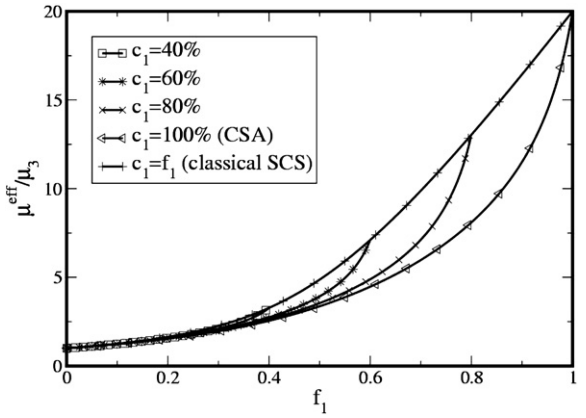

Fig. 3. Dependence of the normalized effective shear modulus on the particle volume fraction for different values of the average mean distance between nearest-neighbor particles ($\mu_{inc}/\mu_{mat} = 20$, $\nu_{inc} = 0.2, \nu_{mat} = 0.43$).

from this statement that any 'intrinsic' (instead of 'relative') size effect could only be predicted from the MRP-based approach if some physics-based internal lengths are introduced in the foregoing mechanical treatment. This is investigated now for the case of an interfacial shell of given thickness surrounding the particles.

4. Size effects for a composite with coated particles

Internal length scales are inherent to almost all deformation and damage mechanisms: when mechanical fields are considered at nanoscales, they may have to be taken into account, since specific phenomena occur which can have important consequences on the macroscopic mechanical behavior. Illustrative examples of such phenomena occurring in nanoparticle-reinforced polymers whose gyration ratio is of the same order of magnitude as the particle diameter have been modelled in Zaoui et al. (2006) according to an MRP-based treatment similar to the one proposed here, leading to 'intrinsic' size effects. Similar treatments could be developed too by taking into account the superficial energy at the interface between the particles and the surrounding matrix. Alternatively, we address here the problem of size effects deriving from the formation of an interphase between particles and the matrix (see, *e.g.*, Berriot et al., 2002, 2003 or Odegard et al., 2005): this third mechanical phase has specific mechanical properties and the coating thickness t_{int} either is independent of the particle radius, as suggested by some Molecular Dynamics simulations (see Brown et al., 2003), or at least does not depend on it linearly.

For sake of simplicity, all the particles have the same radius R_{inc} and the same interphase thickness t_{int}. Thus, the MRP-based treatment of this problem is quite similar to the one developed in Section 3 except for the fact that coated particles are considered now instead of simple ones. So, two patterns only are necessary now: the first pattern consists in three concentric spheres where the internal inclusion with radius $R_1 = R_{inc}$ is the particle, the internal shell with the thickness $R_2 - R_1 = t_{int}$ is made of the interphase material and the exterior shell, with the thickness $R_3 - R_2$, is constituted with the pure matrix material. The second pattern is filled with the matrix material only. One value of the packing parameter λ only is considered from which pattern concentrations c_1 and $c_2 = 1 - c_1$ are derived. Here again, the investigation could be concerned with the derivation of bounds and of various estimates but, for sake of brievity, it is restricted here to the generalized self-consistent prediction of the size-dependent effective moduli. Like hereabove, this prediction derives from the solution of the two elementary problems depicted in Fig. 4, where the patterns have been embedded in an infinite fictitious matrix which is constituted with the effective medium HEM.

If f_1 and f_2 denote the overall volume fractions of the particles and the interphase, respectively, their relative volume fractions in pattern (1) are $f_1/c_1 = (R_1/R_3)^3$ and $f_2/c_1 = (R_2^3 - R_1^3)/R_3^3$, respectively. Most of the equations of Section 3 are still valid except for the fact that now $j \in [1,3]$ while $\lambda \in [1,2]$ again; in addition, in the first auxiliary problem (problem [P′], say), the inclusion of problem [P] (Appendix A) must be replaced by a coated particle. The solution of [P′] can be found in Hervé and Zaoui (1993) (see hereafter). As for the second

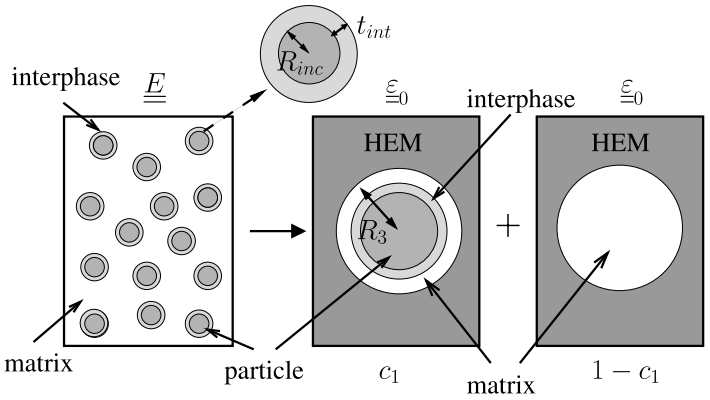

Fig. 4. Size effect modelled with a 2-pattern approach.

auxiliary problem, it still reduces to Eshelby's classical one. Here again, this is not contradictory to the fact that the same auxiliary problems cannot provide any length scale effect when they are integrated into the classical point approaches instead of the proposed MRP-based approach.

Eqs. (4)–(9) are still valid with $j \in [1,3]$ while Eqs. (10) and (11) read now

$$A_{dj}^{(1)} = a'_{dj}, \qquad A_{sj}^{(1)} = a'_{sj}, \qquad j \in [1,3] \tag{14}$$

and

$$\left.\begin{aligned} &A_{d1}^{(2)} = A_{s1}^{(2)} = A_{d2}^{(2)} = A_{s2}^{(2)} = 0 \\ &A_{d3}^{(2)} = 1 + \beta^{\text{eff}} \tfrac{\mu_3 - \mu^{\text{eff}}}{\mu^{\text{eff}}}, \qquad A_{s3}^{(2)} = 1 + \alpha^{\text{eff}} \tfrac{k_3 - k^{\text{eff}}}{k^{\text{eff}}} \\ &\beta^{\text{eff}} = \tfrac{6(k^{\text{eff}}+2\mu^{\text{eff}})}{5(3k^{\text{eff}}+4\mu^{\text{eff}})}, \qquad \alpha^{\text{eff}} = \tfrac{3k^{\text{eff}}}{3k^{\text{eff}}+4\mu^{\text{eff}}} \end{aligned}\right\} \tag{15}$$

As for a'_{dj} and a'_{sj}, $j \in [1,3]$, their expression is a bit too long to be reproduced here but they derive straightforwardly from Eqs. (34) and (36) of Hervé and Zaoui (1993) with use of Eqs. (15), (16), (31) and (32) of the same reference and decomposition of the prescribed uniform strain $\underline{\underline{\varepsilon}}_0$ into its dilational and deviatoric parts.

Before reporting on a few applications of this model in Section 6, some comments are proposed now on simplified versions of this two-pattern MRP-based approach for limiting cases and on their connection with classical micromechanical models.

5. Simplified models for limiting cases

We have strongly stressed the fact that classical micromechanical models deriving from the 'point approach' such as the Mori-Tanaka or the *n*-phase models cannot be considered as relevant ones for the modeling of packing or size effects in particulate composites since the 'inclusions' which they deal with can in no way, contrary to the MRP-based approach, be assimilited with indivual particles and are only abstract representatives of the whole particle phase. Nevertheless, it is interesting to note that some of these models can be shown to yield predictions which coincide with those derived from the MRP-based approach in definite limiting cases. This is briefly illustrated now for dilute spherical coated particles through an extension of the classical dilute Eshelby model (Eshelby, 1956, 1957) to the case of coated inclusions which is called in the following the 'Dilute Coated-Inclusion Model' (DCIM, Section 5.1). This extension can be improved in a somewhat empirical manner for larger (but still small enough) particle volume fractions by recourse to the so-called 'renormalization' procedure which is commonly used in micromechanics: the corresponding 'Improved Dilute Coated-Inclusion Model' (IDCIM) is described in Section 5.2. Finally, the classical '4-phase

model' can also be recovered as a simplified version of the two-pattern MRP-based approach for definite limiting cases (Section 5.3).

5.1. The dilute coated-inclusion model

For an infinitesimal volume fraction of coated particles, a dilute Eshelby-type approximation can be made, similarly to the classical one which is adopted when the particles are supposed to lie far away enough from one another for the interactions between them to be neglected. In other words, individual particles can be considered as embedded separately in an infinite matrix which is constituted with the matrix material and is subjected to the macroscopic strain $\underline{\underline{E}}$ (or stress $\underline{\underline{\Sigma}}$) at infinity (Fig. 5). This approximation refers to problem [P] of Appendix A where the auxiliary strain $\underline{\underline{\varepsilon}}_0$ must be replaced by the macroscopic strain $\underline{\underline{E}}$ itself; indices 1, 2 and 3 refer to the particle, the interphase and the matrix, respectively, with $R_1 = R_{\text{inc}}$, the particle radius, and $R_2 - R_1 = t_{\text{int}}$, the interphase thickness. Since all the coated particles are assumed to be identical, the interphase volume fraction f_2 derives from f_1 and the radii R_1 and R_2 by the relation $f_2/f_1 = R_2^3/R_1^3 - 1$.

From the general equations for a three-phase material

$$\left.\begin{aligned} &f_1\mathbf{A}_1 + f_2\mathbf{A}_2 + f_3\mathbf{A}_3 = \mathbf{I} \\ &\mathbf{C}^{\text{eff}} = f_1\mathbf{C}_1 : \mathbf{A}_1 + f_2\mathbf{C}_2 : \mathbf{A}_2 + f_3\mathbf{C}_3 : \mathbf{A}_3 \end{aligned}\right\} \tag{16}$$

elimination of $f_3\mathbf{A}_3$ yields

$$\mathbf{C}^{\text{eff}} = \mathbf{C}_3 + f_1(\mathbf{C}_1 - \mathbf{C}_3) : \mathbf{A}_1 + f_2(\mathbf{C}_2 - \mathbf{C}_3) : \mathbf{A}_2. \tag{17}$$

Since all the fourth-order tensors in (17) are isotropic and the concentration tensors $\mathbf{A}_1$ and $\mathbf{A}_2$ refer to problem [P] with $\underline{\underline{\varepsilon}}_0 = \underline{\underline{E}}$, Eq. (22) in Appendix A can be used directly; it leads to the solution

$$\left.\begin{aligned} \mu^{\text{eff}} &= \mu_3 + f_1(\mu_1 - \mu_3)a_{d1} + f_2(\mu_2 - \mu_3)a_{d2} \\ k^{\text{eff}} &= k_3 + f_1(k_1 - k_3)a_{s1} + f_2(k_2 - k_3)a_{s2} \end{aligned}\right\} \tag{18}$$

It could be checked that this DCIM solution conforms with the prediction of the MRP-based model of Section 4 when $f_1 \to 0$.

5.2. The improved dilute coated-inclusions model

A semi-empirical way of extending the validity domain of the DCIM towards larger particle volume fractions can be found in the 'normalization' procedure: it consists in the consideration, in the auxiliary problem of Section 5.1 (see Fig. 5), of the fictitious strain $\underline{\underline{\varepsilon}}_0$ instead of $\underline{\underline{E}}$ and in the determination of this variable from the condition $\underline{\underline{E}} = \langle\underline{\underline{\varepsilon}}\rangle$, according to a treatment which is quite similar to the one already used in Eq. (8).

It is easy to find that the resulting effective moduli, which were given by Eq. (18) for the DCIM, read now

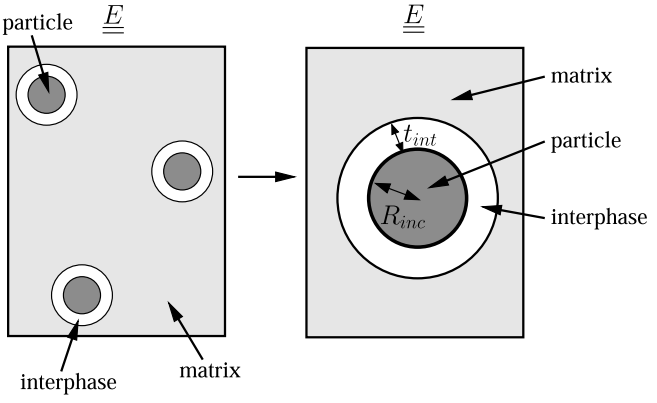

Fig. 5. Definition of the DCIM procedure.

$$\left.\begin{aligned}\mu^{\text{eff}} &= \mu_3 + \frac{f_1(\mu_1-\mu_3)a_{d1}+f_2(\mu_2-\mu_3)a_{d2}}{f_3+f_1a_{d1}+f_2a_{d2}}\\ k^{\text{eff}} &= k_3 + \frac{f_1(k_1-k_3)a_{s1}+f_2(k_2-k_3)a_{s2}}{f_3+f_1a_{s1}+f_2a_{s2}}\end{aligned}\right\} \tag{19}$$

It will be checked in the illustrative applications of Section 6 that the IDCIM predictions significantly improve on the DCIM ones and make them lie much closer to those derived from a 2-pattern treatment.

5.3. The 4-phase model

When studying packing effects in Section 3, we already noticed (see Fig. 3) that a CSA-type behavior (*i.e.*, a behavior ruled by the 3-phase model (Christensen and Lo, 1979) when a self-consistent treatment is chosen) is recovered from the 2-pattern approach when $c_1 = 1$. A similar conclusion can be drawn with the 4-phase model (Hervé and Zaoui, 1993) when coated particles are dealt with (see Fig. 6). Though the physical meaning of the condition $c_1 = 1$ looks quite debatable for monodisperse particles and the basic irrelevance of this kind of 'point approach' model has already been stressed for the analysis of size effects, the corresponding estimates can be considered as reference solutions for larger values of c_1. This is illustrated in Section 6 in view of comparisons.

Let R_1, R_2 and R_3 be, respectively, the radius of the three different spheres in the composite sphere in Fig. 6 by beginning the numbering from the center of the composite sphere. Note that R_1 and $R_2 - R_1$ have now nothing to do with R_{inc} and t_{int}, respectively; they are determined by the phase volume fractions only, through the relations

$$\left(\frac{R_1}{R_3}\right)^3 = f_1, \quad \left(\frac{R_2}{R_3}\right)^3 = f_1 + f_2. \tag{20}$$

The effective moduli k^{eff} and μ^{eff} are then determined straightforwardly from Eqs. (46) and (51) of Hervé and Zaoui (1993).

6. Illustrative applications to coated particle reinforced composites

6.1. Compared predictions

Illustrative examples of the compared predictions of the hereabove described models for the particle size-dependence of the overall moduli of isotropic composites with coated spherical particles are reported now. Here, (1) still refers to the particles, (2) to the interphase and (3) to the matrix. The Poisson ratios and the particle and matrix shear moduli are the following: $\nu_1 = 0.2$, $\mu_1/\mu_3 = 20$, $\nu_2 = 0.47$ and $\nu_3 = 0.43$. The interphase can be either softer ($\mu_2/\mu_3 = 0.5$, (a)-type figures) or harder ($\mu_2/\mu_3 = 2$, (b)-type figures) than the matrix.

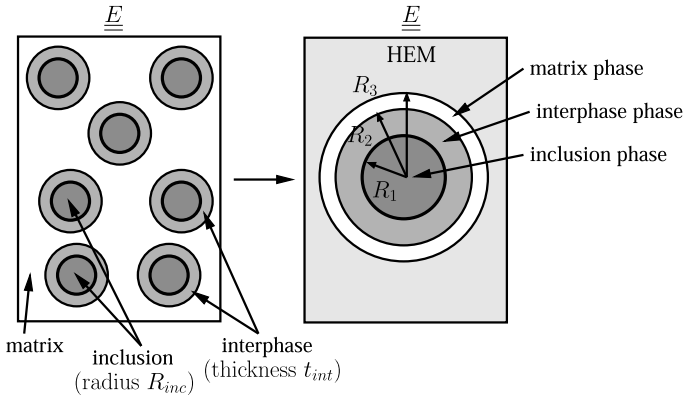

Fig. 6. The 4-phase model.

The following estimates and bounds have been computed: DCIM, IDCIM and 4-phase model estimates; classical Hashin–Shtrikman lower bound (HS^{--}); 2-pattern MRP-based Hashin–Shtrikman-type lower (HSZ^{--}) and upper (HSZ^{+}) bounds, for $c_1 = 50\%$, 60% and 74% (the label 'HSZ' refers to Hervé et al. (1991) where the first MRP-based Hashin–Shtrikman bounds have been derived for the CSA); 2-pattern MRP-based self-consistent estimates for $c_1 = 50\%$, 60% and 74% (2-SC).

The effective bulk and shear moduli have been computed as a function of R_{inc}/t_{int} for various volume fractions of the particles. All the results are very close to each other when the particle volume fraction is small enough, *e.g.*, for $f_1 = 5\%$ in Fig. 7.

For sake of clarity, characteristic results on the normalized effective shear modulus only are reported hereafter for a rather large particle volume fraction ($f_1 = 40\%$), in order to emphasize the differences between the model predictions (Figs. 8 and 9).

Several comments can be made about these results:

- All the reported curves exhibit a particle size-dependence of the overall moduli; nevertheless, it must be stressed that, while all the results have been plotted against the parameter R_{inc}/t_{int}, this variable makes unambiguous sense for the two-pattern MRP-based models and bounds only. For the other models, the pertinent variable in abscissa would rather have been in general, according to Eq. (20), the root of the cubic equation

$$\frac{x^3}{(1+x)^3} = \frac{f_1}{f_1 + f_2}$$

  which only depends of the volume fractions f_1 and f_2 (actually on f_1/f_2).
- As expected, for a fixed coating thickness, when the interphase is stiffer (resp. softer) than the matrix, the smaller the particle size, the larger (resp. smaller) the overall moduli.
- As expected too, the DCIM yields very bad results for the large value of f_1 (40%) considered here and, contrary to the IDCIM, it even violates the classical Hashin–Shtrikman lower bound.
- The 4-phase model predictions are all the more far from the ones derived from the two-pattern model that the second pattern volume fraction ($c_2 = 1 - c_1$) is larger; at the same time, the smaller c_1, the stiffer the overall behavior.
- It can be noticed that too small values of R_{inc}/t_{int} are excluded since they would lead the condition $f_1 + f_2 \leqslant c_1$ to be violated, as discussed in more detail in Section 6.2 below.
- All the 2-pattern predictions for the case (a) of a softer interphase have been gathered in Fig. 10 for $c_1 = 50\%$, 60% and 74%, *i.e.*, both Hashin–Shtrikman-type (upper and lower) bounds and self-consistent estimates: the three sets of three curves, namely (HSZ^{+}), (2-SC) and (HSZ^{--}) are well-separated.

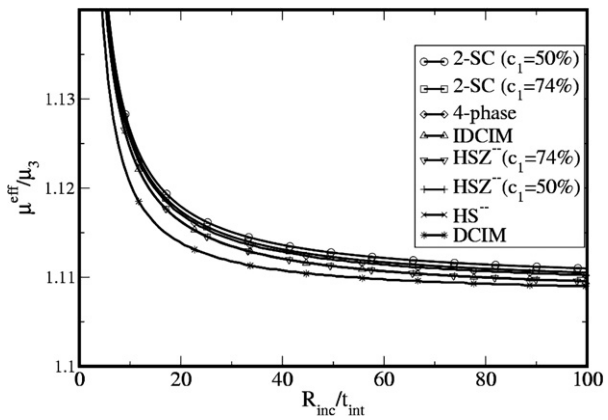

Fig. 7. Normalized shear modulus, $f_1 = 5\%$; case (b).

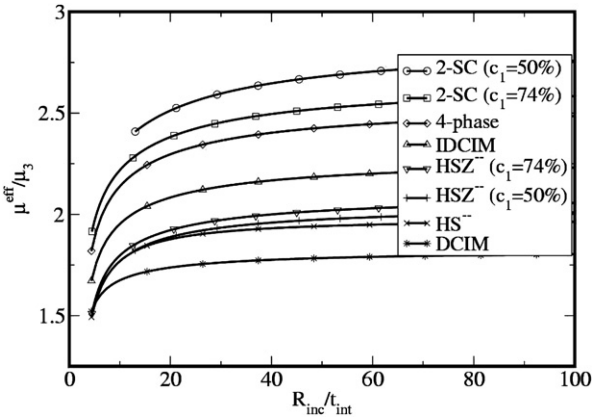

Fig. 8. Normalized shear modulus, $f_1 = 40\%$; case (a).

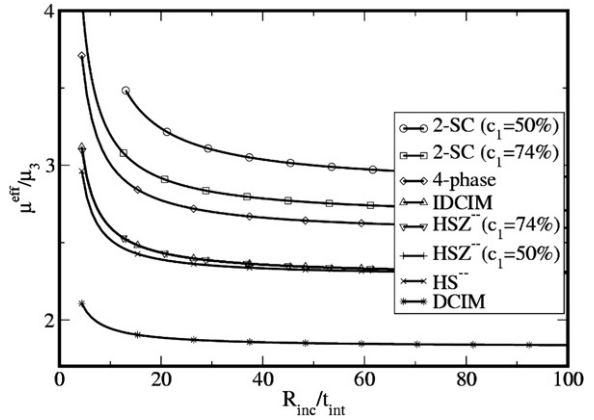

Fig. 9. Normalized shear modulus, $f_1 = 40\%$; case (b).

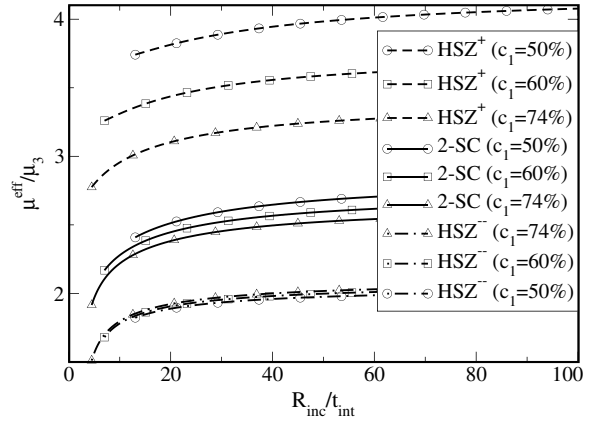

Fig. 10. 2-pattern MRP-based bounds and estimates for the normalized shear modulus, $f_1 = 40\%$; case (a).

Similarly, as expected from Fig. 8, the 4-phase prediction would lie below the (2-SC) set and above the (HSZ^{--}) set. Its precise location depends on the chosen values of the moduli and of the second pattern volume fraction c_2.

6.2. Correlated interphase thickness and particle size

Up to now, the coating thickness and the particle radius have been considered as independent parameters. Nevertheless, the proposed model can be used to investigate situations when these parameters are correlated. For illustration, a power law relation $t_{\text{int}}/t_0 = (R_{\text{inc}}/R_0)^a$ is considered now, with t_0 and R_0 normalization lengths. The associated dependence of the normalized effective shear moduli on the normalized particle radius R_{inc}/R_0, as predicted by a 2-pattern generalized self-consistent scheme with $c_1 = 74\%$, is plotted in Fig. 11a and b for $f_1 = 5\%$ and in Fig. 12a and b for $f_1 = 40\%$, where (a) and (b) still refer to a relatively soft and stiff interphase, respectively, for several values of the exponent a. It is apparent here that the particle size-dependence of the overall moduli vanishes only for $a = 1$, *i.e.*, when the coating thickness is proportional to the particle radius.

Note that some R_{inc}/R_0 values have had to be excluded for preventing any overlap of the coated particles ($f_1 + f_2 \leqslant c_1$). Using Eq. (20), it can be shown that the (positive) R_{inc}/R_0 values must obey the conditions

$$\left.\begin{array}{ll} \dfrac{R_{\text{inc}}}{R_0} \geqslant \left[\dfrac{R_0}{t_0}\left(\left(\dfrac{c_1}{f_1}\right)^{\frac{1}{3}} - 1\right)\right]^{\frac{1}{a-1}} & \text{if} \quad a < 1 \\ \dfrac{R_{\text{inc}}}{R_0} \leqslant \left[\dfrac{R_0}{t_0}\left(\left(\dfrac{c_1}{f_1}\right)^{\frac{1}{3}} - 1\right)\right]^{\frac{1}{a-1}} & \text{if} \quad a > 1 \end{array}\right\} \tag{21}$$

7. Conclusion

It has been shown in this paper that, contrary to a common statement, the classical framework of micromechanical modeling can allow some size effects on composite material behavior to be taken into account as soon as the usual 'point approach' is given up in favor of a refined description of the structural morphology such as the one proposed by the 'MRP-based approach'. Whereas, within the point approach, 'inclusions' which may appear in the modeling treatment are abstract representatives of mechanical phases of the composite, taken as a whole, and can in no way be identified with their basic constitutive inhomogeneities, the MRP-based approach makes it possible to consider individual particles or fibers and to assign them some of their own attributes, such their size, or some characteristic lengths of their packing distribution. This has been illustrated on simple packing and size effects in elastic particulate isotropic composites with monodisperse spherical particles, with special attention paid to the case when an interphase with specific mechanical properties is formed between the particles and the matrix. As already noted, a similar treatment could have been

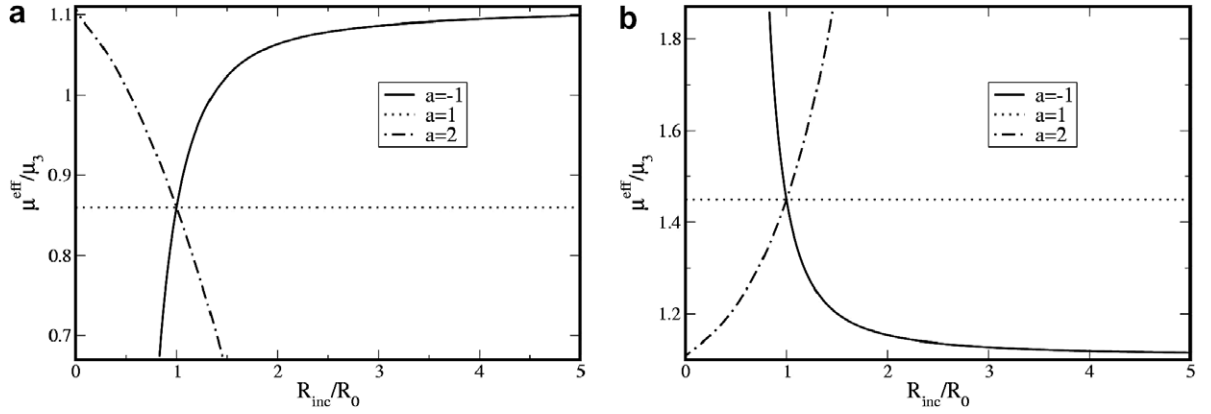

Fig. 11. Particle size dependence of the normalized effective shear modulus as predicted by a two-pattern approach; $f_1 = 5\%$, $c_1 = 74\%$, $R_0/t_0 = 1$.

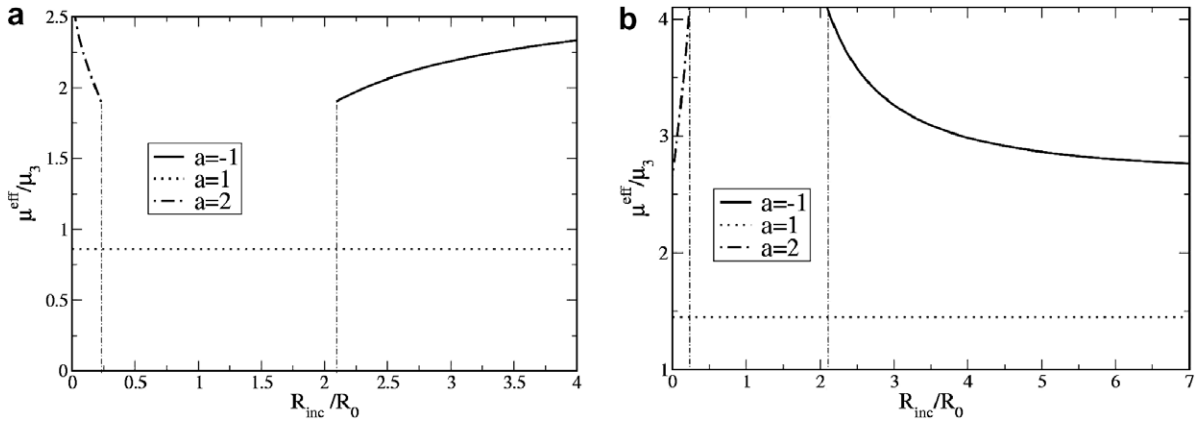

Fig. 12. Particle size dependence of the normalized effective shear modulus as predicted by a two-pattern approach; $f_1 = 40\%$, $c_1 = 74\%$, $R_0/t_0 = 1$.

developed by taking into account an interfacial energy instead of an interphase with finite thickness. Obviously, these results could be easily extended to infinite cylindrical fibers and to transverse isotropy. Though several classical micromechanical models have been shown to yield the same predictions as the MRP-based approach in well-definite limiting cases, the stress must be laid on the basic differences between the concerned approaches and on their quite different vocation for modeling size effets on the overall behavior of heterogeneous materials.

The reported illustrations have been intentionally chosen for their simplicity in order to emphasize the methodology rather than the computational techniques. Nevertheless, the same approach could be used for dealing with more complex situations: for instance, if the exact shape of nanosized fillers is considered as an important feature for the prediction of the filler size-dependence of the overall moduli, the elementary problems to be solved according to the MRP-based approach are still defined quite simply whereas a numerical resolution is now necessary, as illustrated in Bornert et al. (1996) where a FEM resolution is used. Similarly, if definite physico-chemical phenomena are known to rule the very short range matrix-filler interactions, they have to be modeled specifically instead of using the idealized picture of a homogeneous interphase shell which has been adopted here for sake of simplicity. Due to this intentional choice of simplicity, direct comparisons with experimental results would not be sensible in the present state of the reported work. Nevertheless it can be mentioned that quite consistent and satisfying quantitative comparisons (Marcadon, 2005) have been performed between the results of Molecular Dynamics simulations of model particle-reinforced nanocomposites and predictions derived from the use of the method proposed in Section 4.

It is apparent too that the simplified version of the MRP-based approach which has been presented and applied hereabove has a limited capacity only to model size effects, since, *e.g.*, it can yield identical predictions for distinct characteristics of the size distribution of the particles. New developments of the method which are still in progress are expected to improve its modeling ability and to broaden the field of its possible applications.

Acknowledgements

Dr M. Bornert (LMS, Ecole Polytechnique/CNRS, France) is gratefully acknowledged for his leading role in the numerical implementation of the models and bounds derived from the MRP-approach. We are also indebted to Pr N. Albérola, Pr D. Brown and Dr P. Mélé (LMOPS, Chambéry, France) for many fruitful discussions.

Appendix A. 'Problem [P]': the coated spherical inhomogeneity

The solution of the classical problem of a coated spherical inhomogeneity (referred to as 'Problem [P]' in the main text), is recalled here for use in the models proposed in the paper: a spherical inhomogeneity (radius R_1, elastic shear and bulk moduli μ_1 and k_1), surrounded by a concentric shell (thickness $t = R_2 - R_1$, elastic shear and bulk moduli μ_2 and k_2), is embedded in an infinite homogeneous matrix (phase (3), elastic shear and bulk moduli μ_3 and k_3), subjected to homogeneous strain conditions $\underline{\underline{\varepsilon}}_0$ at infinity (see Fig. 13).

Following Hervé–Zaoui's derivation (Hervé and Zaoui, 1990), uniform dilatational ($\theta_0/3\underline{\underline{i}}$) and deviatoric ($\underline{\underline{e}}_0$) strain conditions can be prescribed separately at infinity. Let $\theta_i/3\underline{\underline{i}}$ and $\underline{\underline{e}}_i$ be the average dilatational and deviatoric strain tensors in phase (i) ($i \in [1,2]$), respectively. They are related to the prescribed strain by the relations

$$\left.\begin{aligned} \theta_i &= a_{si}\theta_0 \\ \underline{\underline{e}}_i &= a_{di}\underline{\underline{e}}_0 \end{aligned}\right\} i \in [1,2] \tag{22}$$

with (Hervé and Zaoui, 1990)

$$\left.\begin{aligned} a_{s1} &= \frac{(3k_3+4\mu_3)(3k_2+4\mu_2)}{(3k_2+4\mu_3)(3k_1+4\mu_2)+12c(\mu_3-\mu_2)(k_2-k_1)} \\ a_{s2} &= \frac{(3k_3+4\mu_3)(3k_1+4\mu_2)}{(3k_2+4\mu_3)(3k_1+4\mu_2)+12c(\mu_3-\mu_2)(k_2-k_1)} \\ a_{d1} &= 225(1-\nu_3)(1-\nu_2)X_0\,\frac{-4(X_0-1)[\eta_1 c^{7/3}-\eta_2(7-10\nu_2)]+35(1-\nu_2)\eta_2}{\Delta} \\ a_{d2} &= \frac{15(1-\nu_3)X_0}{1-c} \\ &\quad \frac{(X_0-1)\{A+60c(1-\nu_2)[\eta_1 c^{7/3}-\eta_2(7-10\nu_2)]\}+35(1-\nu_2)\eta_2\eta_3(1-c)}{\Delta} \end{aligned}\right\} \tag{23}$$

and, with ν_i the Poisson ratio of phase i, $i \in [1,3]$,

$$\left.\begin{aligned} c &= \left(\frac{R_1}{R_2}\right)^3 \\ X_0 &= \frac{\mu_3}{\mu_2} \\ \alpha &= \frac{\mu_1}{\mu_2} - 1 \\ \eta_1 &= (49 - 50\nu_1\nu_2)\alpha + 35(1+\alpha)(\nu_1 - 2\nu_2) + 35(2\nu_1 - \nu_2) \\ \eta_2 &= (7+5\nu_1)(1+\alpha) + 4(7-10\nu_1) \\ \eta_3 &= 2(1+\alpha)(4-5\nu_2) + 7 - 5\nu_2 \\ A &= -4[\eta_3 - 2\alpha(4-5\nu_2)c][\eta_1 c^{7/3} - \eta_2(7-10\nu_2)] - 126\alpha\eta_2 c(1-c^{2/3})^2 \\ C &= -[\eta_3 + \alpha(7-5\nu_2)c][4\eta_1 c^{7/3} + \eta_2(7+5\nu_2)] - 126\alpha\eta_2 c(1-c^{2/3})^2 \\ \Delta &= [2(4-5\nu_3)C + (7-5\nu_3)AX_0](X_0-1) + \ldots \\ &\quad \ldots 525\eta_2(1-\nu_2)[2\alpha(\nu_2-\nu_3)c + (1-\nu_3)\eta_3]X_0 \end{aligned}\right\} \tag{24}$$

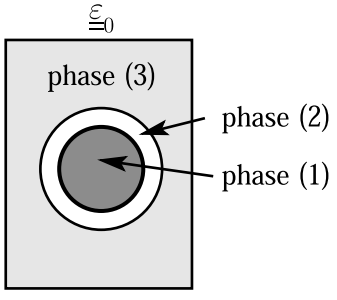

Fig. 13. Problem [P].

References

Berriot, J., Lequeux, F., Monnerie, L., Montes, H., Long, D., Sotta, P., 2002. Filler-elastomer interaction in model filled rubbers; a H NMR study. Journal of Non-Crystalline Solids, 719–724.

Berriot, J., Martin, F., Montes, H., Monnerie, L., Sotta, P., 2003. Reinforcement of model filled elastomers; characterization of the cross-licking density at the filler-elastomer interface by H NMR measurements. Polymer 44, 1437–1447.

Bornert, M., Stolz, C., Zaoui, A., 1996. Morphologically representative pattern-based bounding in elasticity. Journal of the Mechanics and Physics of Solids 44 (3), 307–331.

Brown, D., Mélé, P., Marceau, S., Albérola, N.D., 2003. A molecular dynamics study of a model nanoparticle embedded in a polymer matrix. Macromolecules 36, 1395–1406.

Christensen, R.M., Lo, K.H., 1979. Solution for effective shear properties in three-phase sphere and cylinder models. Journal of the Mechanics and Physics of Solids 27, 315–330.

Eshelby, J.D., 1956. The continuum theory of lattice defects. In: Seitz, F., Turnbull, D. (Eds.), . In: Prog Solid State Phys, 3. Academic Press Inc, pp. 79–144.

Eshelby, J.D., 1957. The determination of the elastic field of an ellipsoidal inclusion, and related problems. Proceedings of the Royal Society of London A421, 376–396.

Hashin, Z., 1962. The elastic moduli of heterogeneous materials. Journal of Applied Mechanics 29, 143–150.

Hashin, Z., Shtrikman, S., 1963. A variational approach to the theory of the elastic behavior of multiphase materials. Journal of the Mechanics and Physics of Solids 11, 127–140.

Hervé, E., Stolz, C., Zaoui, A., 1991. A propos de l'assemblage des sphères composites de Hashin. Comptes Rendus de l'Académie des Sciences 213 (Série II), 857–862.

Hervé, E., Zaoui, A., 1990. Modelling the effective behavior of nonlinear matrix-inclusion composites. European Journal of Mechanics A/Solids 9 (6), 505–515.

Hervé, E., Zaoui, A., 1993. n-layered inclusion-based micromechanical modelling. International Journal of Engineering and Sciences 31 (1), 1–10.

Kröner, E., 1978. Self-consistent scheme and graded desorder in polycristal elasticity. Journal of Physics F8, 2261–2267.

Marcadon, V., 2005. Effets de taille et d'interphase sur le comportement mécanique de nanocomposites particulaires. PhD Thesis, Ecole Polytechnique, France.

Mori, T., Tanaka, K., 1973. Average stress and average elastic energy of materials with misfitting inclusions. Acta Metal 21, 571–574.

Odegard, G.M., Clancy, T.C., Gates, T.S., 2005. Modeling of the mechanical properties of nanoparticle/polymer composites. Polymer 46, 553–562.

Stolz, C., Zaoui, A., 1991. Analyse Morphologique et approches variationnelles du comportement d'un milieu élastique hétérogène. Comptes Rendus de l'Académie des Sciences (Série II), Paris 312, 143–150.

Torquato, S., 1995. Mean nearest-neighbor distance in random packings of D-dimensional hard spheres. Physical Review Letters 74, 2156–2159.

Zaoui, A., Marcadon, V., Hervé, E., 2006. Partice size effects in nanocomposites. In: Sun, Q.P., Tong, P. (Eds.), IUTAM Symposium on Size Effects on Material and Structural Behavior at Micron- and Nano-scales. Springer, the Netherlands, pp. 97–106.